Gas-Phase Pyrolyses of 2-Nitropropane and 2-Nitropropanol: Shock-Tube Kinetics

Yi-Xue Zhang and S. H. Bauer*

Department of Chemistry and Chemical Biology, Baker Chemical Laboratory, Cornell University, Ithaca, New York 14853

Received: September 10, 1999; In Final Form: October 29, 1999

The kinetics of the thermal decomposition of 2-nitropropane was investigated in a shock tube over the temperature range 970−1150 K under high dilution in argon at total pressures 4.5−6 atm. The decay of 2-nitropropane and the production of NO_2 were followed spectrophotometrically at 276 and 405 nm, respectively. The unimolecular rate constant deduced from the loss of 2-nitropropane at the high-pressure limit is: $k_\infty = 10^{14.55\pm0.13}\exp\{(-54.2 \pm 3.8\ \text{kcal/mol})/RT\}\ s^{-1}$. The products of pyrolysis were identified and quantified with FTIR and GC. The major products are NO, $CH_3CH{=}CH_2$, CO, CH_3CHO, C_2H_4, and $(CH_3)_2CO$. The decomposition proceeds primarily through C−N bond fission, while the contribution from the five center elimination of HONO accounts for less than 20% of the total loss of 2-nitropropane. A reaction mechanism that consists of 81 elementary steps is proposed; it accounts quantitatively for the overall pyrolysis. Numerical simulations with the mechanism reproduce reasonably well the NO_2 vs time profiles at different temperatures and the distributions of major reaction products over the temperature range studied. When the mechanism was subjected to a sensitivity and principal component analysis, it was found that only 58 reactions in the mechanism are needed to faithfully reproduce the observed product distributions. The fragmentation and reaction sequence in the pyrolysis is graphically presented so that the fundamental chemistry of the overall reaction can be readily visualized. The initial stage of the decomposition of 2-nitropropanol was also investigated following the above experimental protocol. The rate of the pyrolysis appears to be similar to that of the 2-nitropropane over the temperature range studied, but it has a much lower activation energy. The unimolecular rate constant can be expressed as $10^{11.29\pm0.78}\exp\{(-37.5 \pm 3.6\ \text{kcal/mol})/RT\}\ s^{-1}$. No pressure dependence was observed over the pressure range investigated (4−5.3 atm), and therefore it is presumed that the rate constant represents the high-pressure limit. Both the low A factor and the low activation energy suggest the involvement of the OH group in the first step of the reaction. NO_2 production and subsequent consumption during the decomposition was also observed. The reaction products from this species are similar to those of 2-nitropropane.

Introduction

Current high explosives and propellants incorporate multiple NO_2 functional groups.[1,2] The initial steps in the thermal decompositions of these compounds (e.g., hexahydro-1,3,5,-trinitro-*s*-triazine (RDX), 1,3,5,7,-tetranitro-1,3,5,7,-tetraazacyclooctane (HMX), and 1,3,3,-trinitroazetidine (TNAZ)) typically involve the fission or transformation of the weakest C−N bonds.[3−5] But the overall decomposition mechanisms are not clear cut. A systematic study of simple prototype nitro compounds may facilitate the determination of basic bond dissociation energies of the various types of C−N bonds and may reveal the general mechanistic features for the fragmentation sequence of the corresponding nitro compounds. A review of previous investigations of these materials was recently reported by Zhang and Bauer.[6] Herein, we describe an investigation of the thermal decomposition of 2-nitropropane. A brief exploration of the initial stages of the decomposition of 2-nitropropanol is also included. This suggests different routes that might be followed in the thermal decomposition of nitro compounds.

Experimental Section

The shock tube is constructed of stainless steel; its internal diameter is 2.50 cm. The length of the driver and driven sections are 120 and 170 cm, respectively. Shock waves were generated by increasing the pressure of the He driver until a selected Mylar diaphragm broke. Typical pressures in the driver and driven sections were 70 psig and 350−520 Torr, respectively. Two piezoelectric pressure sensors are stationed 10.0 cm apart at the end of the driven section. Their summed signal was recorded and digitized in a Biomation 8100 transient recorder, and then stored in a IBM 386 computer. The accuracy of the recorded time intervals is ±1 μs; this corresponds to an ambiguity of ∼8 K in the reflected shock temperature. The effective residence time under reflected shock conditions (∼1.3 ms) was defined as the elapsed time from the initiation of the reflected shock wave to the time when the pressure signal had decayed to 80% of the initial reflected shock level. The temperature of the reflected shock was estimated according to the computational procedure recommended by Gardiner et al.[7] for very dilute reaction mixtures. The entire shock tube and gas manipulating lines were kept at 130 °C to minimize adsorption of the nitropropanes onto the shock tube walls.

High purity Ar was used as the diluent. 2-Nitropropane (>97%, Aldrich) and 2-nitropropanol (98%, Aldrich) were used without further purification; typical concentrations of these compounds in the shocked mixtures were ∼0.65% (mole fraction). The initial *i*-$C_3H_7NO_2$/Ar and *i*-$C_3H_6(OH)NO_2$/Ar mixtures were prepared in a ∼6 L Pyrex vessel and allowed to

10.1021/jp993204e CCC: $19.00
Published on Web 01/26/2000

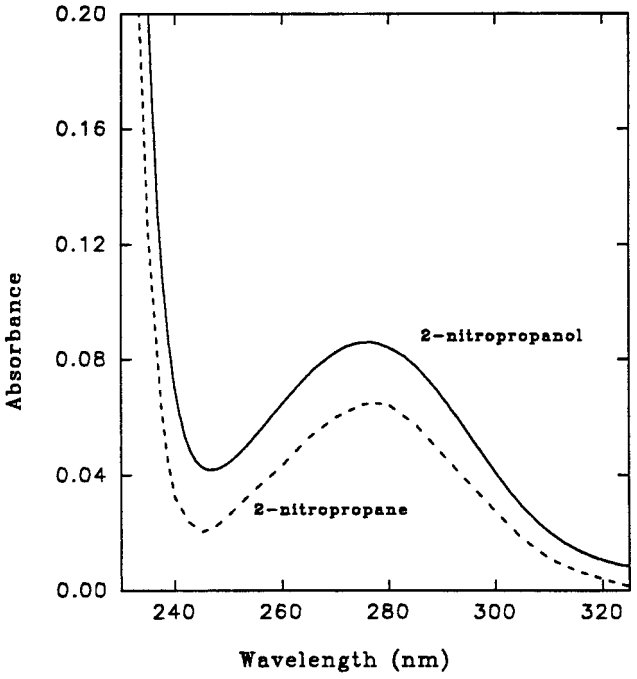

Figure 1. UV spectra of 2-nitropropane (1.936×10^{-3} M) and 2-nitropropanol (1.804×10^{-3} M). The solvent is acetonitrile and cell length is 1 cm.

mix at 130 °C for ~12 h before use. Research grade CO, NO, CH_4, C_2H_6, C_2H_4, $CH_3CH{=}CH_2$, C_3H_8, *i*-C_4H_8, *i*-C_4H_{10}, and CH_3CHO (Aldrich) and a CH_2O solution were used for GC and FTIR calibrations.

Analytical Methods. Changes in the concentrations of *i*-$C_3H_7NO_2$, *i*-$C_3H_6(OH)NO_2$, and NO_2 during the reaction were followed spectrophotometrically by recording their UV absorptions at 276 and 405 nm, respectively. The UV spectra of 2-nitropropane and 2-nitropropanol (both in CH_3CN) were determined with a HP8451A diode array UV−visible spectrometer (Figure 1). Their extinction coefficients at 276 nm (room temperature) are 34 and 46 M^{-1} cm^{-1}, respectively. The extinction coefficient of NO_2 at elevated temperatures was determined by Huffman and Davidson[8] and can be represented by:[9] $\epsilon(M^{-1}\ cm^{-1}) = 179.6 - 0.05475T + 6.33 \times 10^{-6}\ T^2$, at 405 nm, over the temperature range 400−2000 K. UV light emitted from a xenon arc lamp (Oriel) was directed normal to the axis of the shock tube through a quartz extension attached to the end of the shock tube. The quartz cylinder was partially aluminized so that the incoming light is internally reflected several times before leaving the tube. The effective path length (13 cm) was determined using diacetyl-Ar mixtures of known concentration at 310 nm (extinction coefficient is 15 at 298 K). The multiple pass configuration greatly enhances the sensitivity of the UV absorption measurements. Details of the construction of this extension have been described previously.[9]

Three methods were used to identify and quantify the reaction products. Some of the compounds were identified by GC/MS and GC/FTIR. Samples extracted from the terminal end of the tube after the shock heated gas was quenched were analyzed with a Polaris FTIR spectrometer (Matheson Instruments, Inc). Integrated peak areas were used to determine quantitatively the concentrations of CO and NO. Beer's law proved valid for these species over the concentration range encountered in this work. A typical spectrum of a product mixture is shown in Figure 2. The major contribution to the CO_2 peak is the residual CO_2 in the FTIR chamber. Immediately after each shock, a 16 mL sample at a known pressure was collected through the sampling valve at the end of the driven section of the shock tube. A small portion of this sample was then injected into the GC column through a six-port valve for analysis. An HP 18790 chromatograph with a thermal conductivity detector was used to separate and determine the concentrations of products using a 30 ft × 1/8 in. stainless steel tube packed with Hayesep DB 100/120. The flow rate of the carrier gas (He) was typically 25 mL/min. The column temperature was held at 25 °C for the first 5 min and then ramped at a rate of 12 °C/min until it reached the final temperature 240 °C. The following major reaction products were identified: CH_4, C_2H_4, CH_2O, $CH_3CH{=}CH_2$, CH_3CHO, $(CH_3)_2CO$. Traces of CH_3CN, C_3H_8, *i*-C_4H_{10}, *i*-C_4H_8, and C_2H_6 were also formed.

Results

The unimolecular rate constant for the initial decay rate of 2-nitropropane was derived from first order plots of absorption intensity loss, recorded spectrophotometrically at 276 nm, during the early part of the reaction. A typical experimental scan is shown in Figure 3a, b. The initial rapid increase in absorbance was due to the sudden jump in temperature and pressure of the reaction mixture upon the arrival of the incident and reflected shock waves. In most runs the logarithm of the absorbance vs time at 276 nm was linear up to 80% completion of the reaction and then decreased further with a lesser slope. The Arrhenius plot of k_{uni} obtained from early parts of the 2-nitropropane decay curves is shown in Figure 4. That rate constant can be expressed as

$$k_{uni} = 10^{14.55\pm0.13} \exp\{(-54.2 \pm 3.8\ \text{kcal/mol})/RT\}\ s^{-1} \quad (1)$$

Since no pressure dependence was observed, we assume that the rate constant is at the high-pressure limit. The reported k_{uni} by Glänzer and Troe[10] is $10^{15.5}$ exp{(−54 kcal/mol)/*RT*} s^{-1}. While their activation energy is close to that in eq 1, their *A* factor is larger by a factor of 10. They proposed that C−NO_2 bond fission was the predominant fragmentation step, over this temperature range, while the contribution from elimination of HONO is small.

NO_2 is an important intermediate in the decomposition of nitro compounds. A clear understanding of its kinetics is crucial for elucidating the mechanism of the overall conversion. We monitored the NO_2 concentration vs time during the decomposition under a variety of experimental conditions. Typical results are shown in Figures 5 and 6. The NO_2 profiles resemble those observed in the decomposition of nitromethane, suggesting similarities in the mechanisms of the two systems. At the lower temperatures, NO_2 was produced and consumed relatively slowly; whereas at higher temperatures both processes were very fast. The final NO_2 concentrations were very low, both for low and high-temperature runs. This is consistent with the FTIR spectra of the product mixtures, which show no NO_2 peak. The dotted lines in the figures are computer simulations described below.

The distributions of the major products over the experimental temperature range are presented in Figures 7−9. As reported previously for the low-temperature decompositions, $CH_3CH{=}CH_2$ and NO are the most abundant species. Roughly half of the original 2-nitropropane is converted to propylene. There appeared traces of CH_3CN, C_2H_6, C_3H_8, and C_4H_{10} in the final mixture, but their concentrations were not quantitatively determined. HONO and HCN were not found in the quenched reaction mixtures. The solid lines in the figures were derived by numerical simulations as described below.

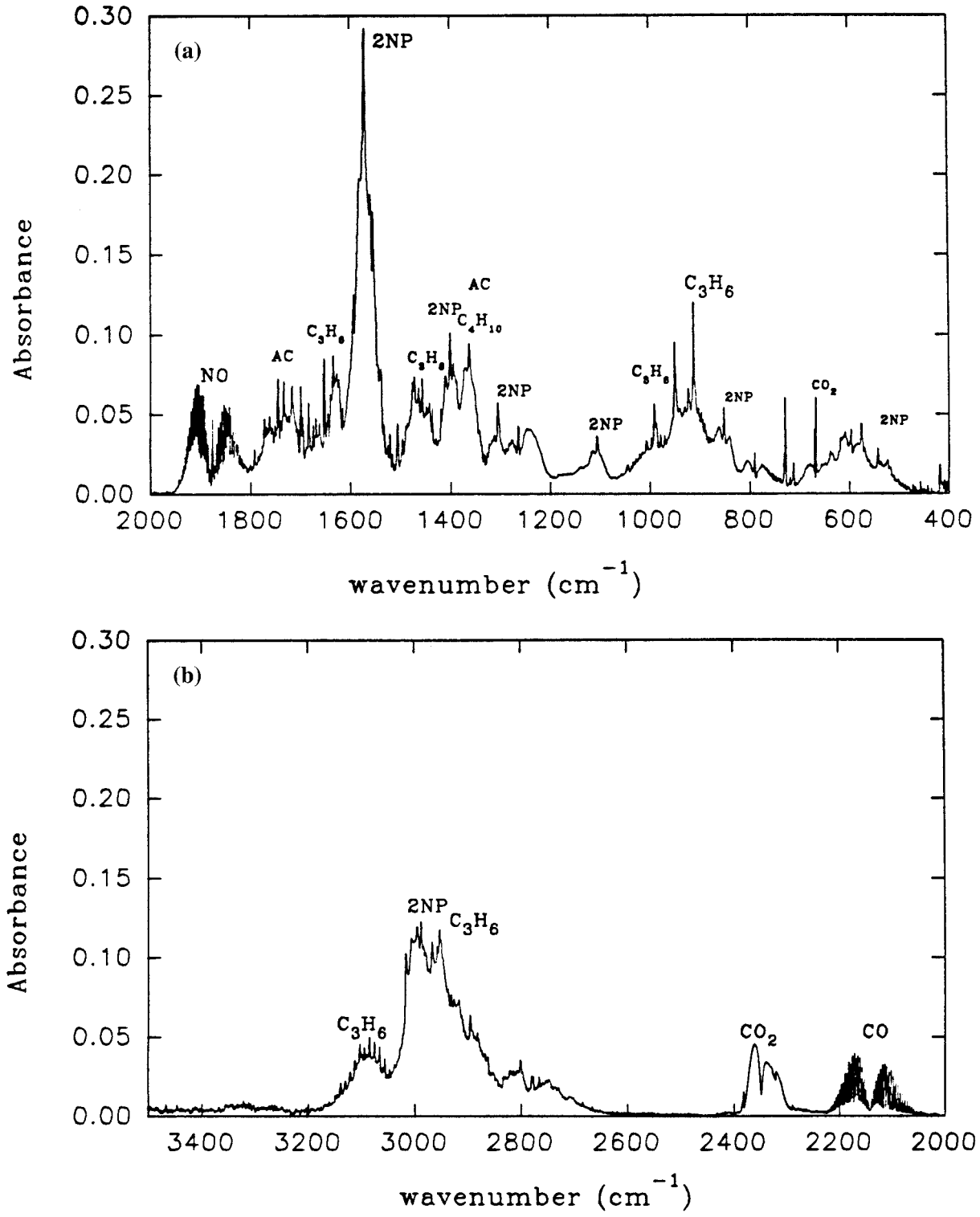

Figure 2. FTIR spectra of the quenched mixture of products developed during 1.3 ms residence time under reflected shock conditions, for 2-nitropropane. Conditions: $T = 1020$ K, $P = 5$ atm Ar; $[i\text{-}C_3H_7NO_2]_o = 4.9 \times 10^{-7}$ mol/cm^3. Acetone is abbreviated as AC in the figure.

The thermal decomposition of 2-nitropropanol was also investigated; the same procedures were followed. The UV absorption of 2-nitropropanol at 276 nm was recorded, from which unimolecular rate constants were estimated. A typical kinetic curve for this compound is shown in Figure 10. Note that during the later part of the reaction, the recorded values deviate considerably from first order, indicating either that the reaction was slowed by some of the secondary reactions or that some of the products also absorb strongly in this region. The initial rates of the reaction were used to determine the Arrhenius parameters for the decomposition. The derived unimolecular rate constant (see Figure 11) can be expressed as

$$k_{uni} = 10^{11.29\pm0.78} \exp\{(-37.5 \pm 3.6 \text{ kcal/mol})/RT\} \text{ s}^{-1} \quad (2)$$

NO_2 accumulation and its subsequent consumption were observed at 405 nm for the tested temperature range. GC analysis of postshock mixtures shows compositions quite similar to those generated in the 2-nitropropane system. However, quantitative determinations of product distributions were not attempted.

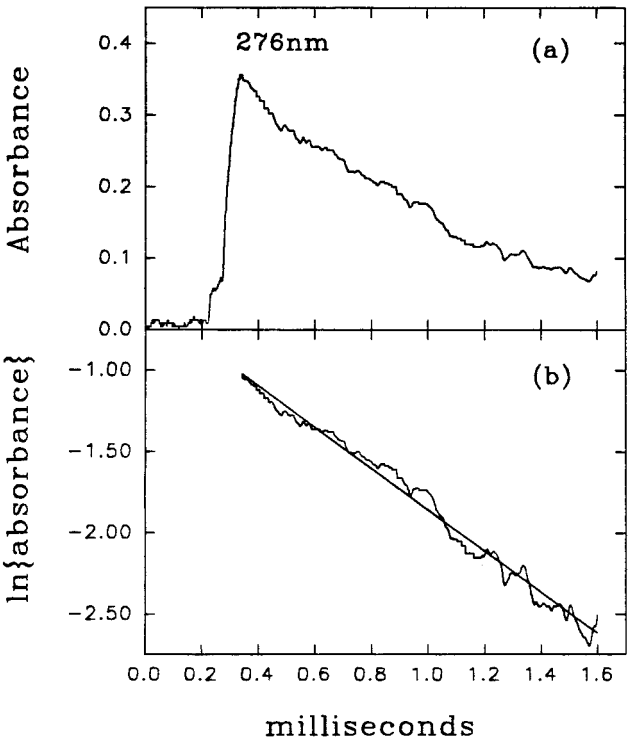

Figure 3. (a) Absorbance vs time (276 nm) during the thermal decomposition i-$C_3H_7NO_2$ at 1050 K. The first and second rises in absorbance are due to the density and temperature increases developed by the incident and reflected shock waves, respectively. Total pressure = 5 atm. $[i\text{-}C_3H_7NO_2]_o = 5.0 \times 10^{-7}$ mol/cm^3. (b) The logarithm of absorbance for of 2-nitropropane vs time at 276 nm.

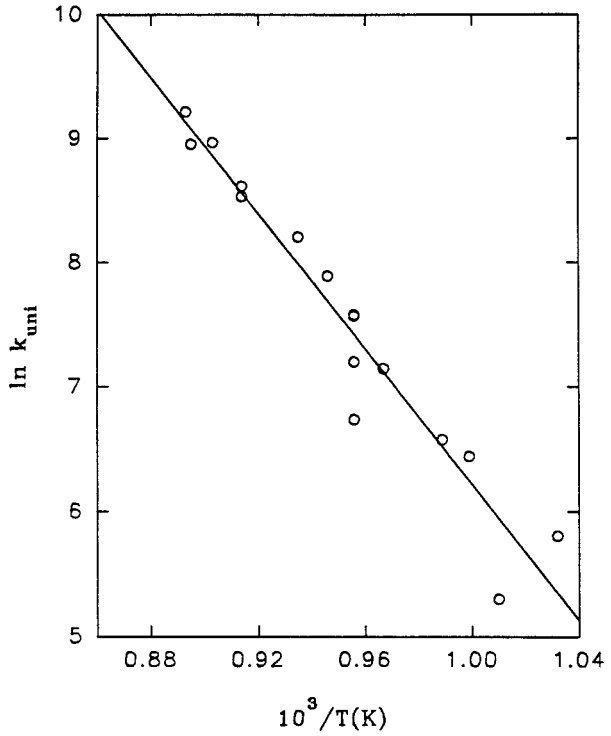

Figure 4. Arrhenius plot of the derived rate constants, for 2-nitropropane. Total pressures at reflected shock conditions are 4.5−5.5 atm. $[i\text{-}C_3H_7NO_2]_o$ is $4.5 \times 10^{-7} - 5.5 \times 10^{-7}$ mol/cm^3. Symbols are experimental values and the solid line is the least-squares fit of the data.

Discussion

The thermal decompositions of aliphatic nitro compounds have been extensively investigated over the past few decades.

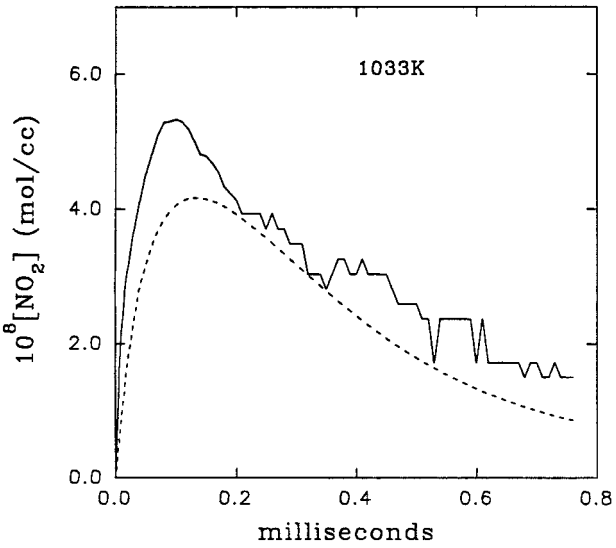

Figure 5. Solid line: scaled recorded $[NO_2]$ vs time for 2-nitropropane. Conditions: $T = 1033$ K, $P = 5.2$ atm, $[i\text{-}C_3H_7NO_2]_o = 5.0 \times 10^{-7}$ mol/cm^3. The dashed line is the computed $[NO_2]$ vs time, per the mechanism in Table 1.

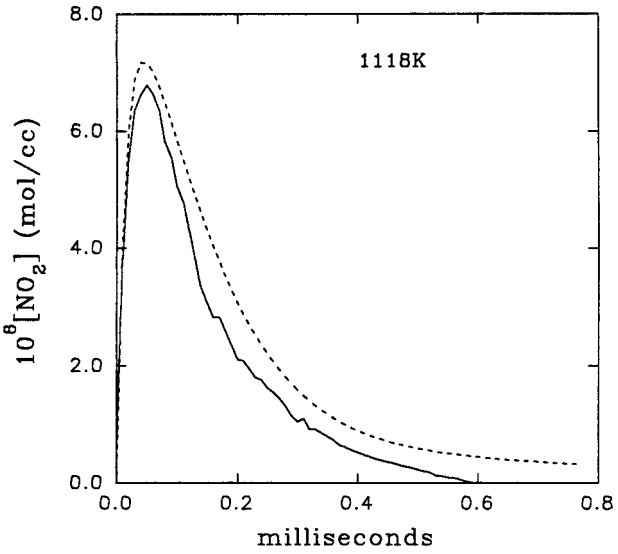

Figure 6. Solid line: scaled recorded $[NO_2]$ vs time for 2-nitropropane. Conditions: $T = 1118$, $P = 5.6$ atm, $[i\text{-}C_3H_7NO_2]_o = 5.0 \times 10^{-7}$ mol/cm^3. The dashed line is the computed $[NO_2]$ vs time, per the mechanism in Table 1.

The early studies were summarized by Nazin et al.[11,12] Recent investigations with shock-tube[10,25] and molecular beam techniques[13] refined the unimolecular rate constants and provided convincing experimental evidence for multiple pathways for the initiation of these reactions. Three elementary reactions have been invoked by various researchers to explain their experimental results: (1) C−NO_2 bond fission; (2) HONO elimination (when a β-H is available); (3) C−NO_2 to C−ONO isomerization. Other energetically unfavorable reactions such as HNO elimination with an H from the geminal position, e.g., $CH_3NO_2 \rightarrow CH_2O + HNO$ and i-$C_3H_7NO_2 \rightarrow (CH_3)_2CO + HNO$, and the loss of oxygen from the nitro group, e.g., $CH_3NO_2 \rightarrow CH_3NO + O$, were also postulated.

The thermal decomposition of 2-nitropropane was studied by Frejacquens,[14] Smith and Calvert,[15] and Waddington and Warriss[16] in static reactors, and by Wilde[17] in a flow system. The temperature and pressure ranges in these studies were 411−713 K and 4−40 Torr, respectively. They found that the

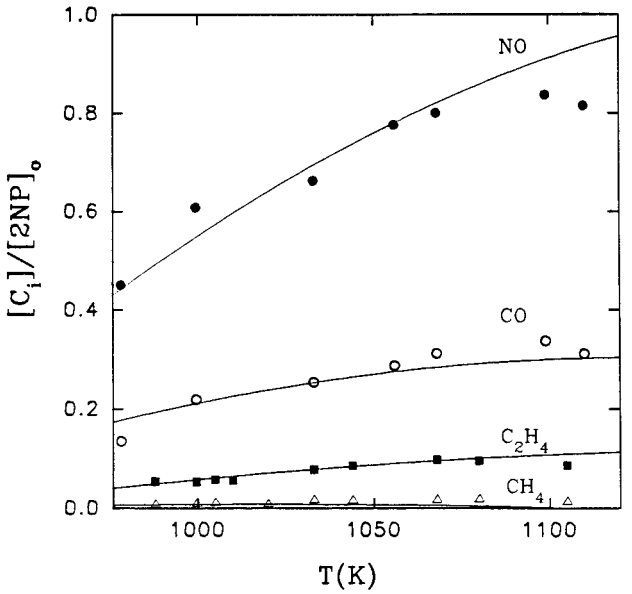

Figure 7. Observed vs computed product distributions developed during the thermal decomposition of 2-nitropropane. The symbols are experimental values and the solid lines are based on numerical simulations, per the mechanism in Table 1.

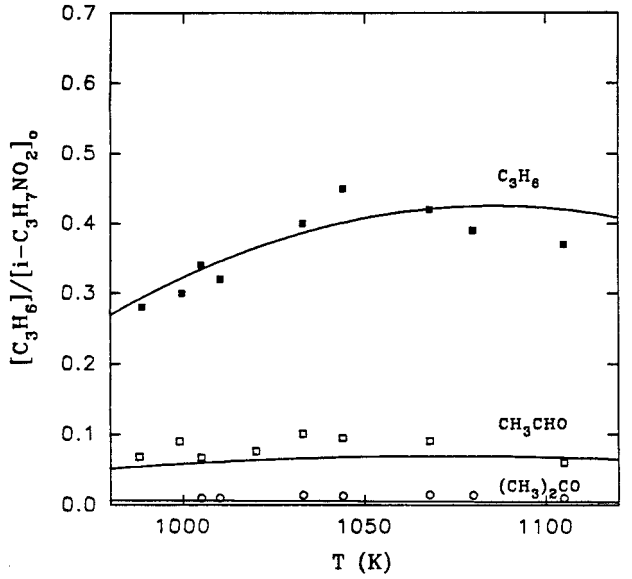

Figure 8. Observed vs computed product distributions developed during the thermal decomposition of 2-nitropropane. The symbols are experimental values and the solid lines are based on numerical simulations, per the mechanism in Table 1.

pyrolysis follows first order kinetics. The rate constants deduced in these investigations were mutually consistent, with *A* factors in the range 11−11.3 and activation energies in the range 37.67−39.3 kcal/mol. Spokes and Benson[18] described a very low-pressure pyrolysis experiment with 1-nitro- and 2-nitropropanes. They adjusted the above magnitudes to 11.3 ± 0.2 and 40 ± 0.5 kcal /mol, respectively. Although the derived kinetic parameters from the above investigations were very similar, the product distributions were not. Clearly, the reactor surfaces considerably affected the rates and the mechanisms of pyrolysis. For example, Smith and Calvert[15] found that packing the reactor with Pyrex wool increased the rate of the reaction so that water, acetonitrile, and acetone became the most abundant products instead of propylene and nitric oxide. This is also an indication that free radicals are actively involved in these conversions. The effect of the reactor surface was further

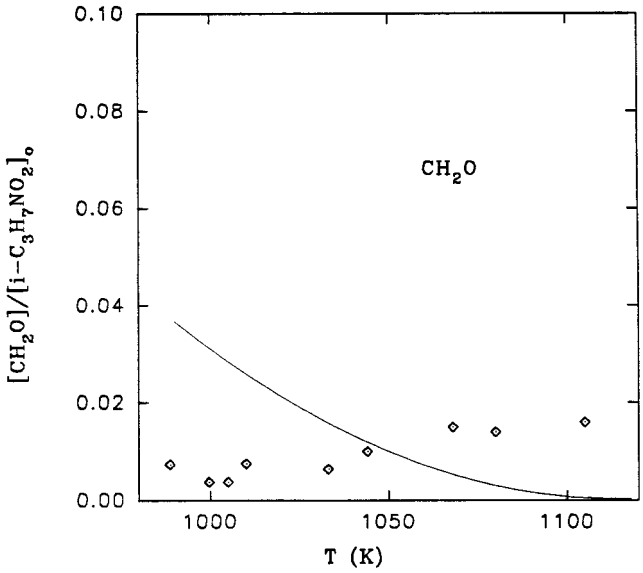

Figure 9. The measured formaldehyde levels (of questionable precision) developed during the thermal decomposition of 2-nitropropane (symbols). The solid line was based on numerical simulations, per the mechanism in Table 1.

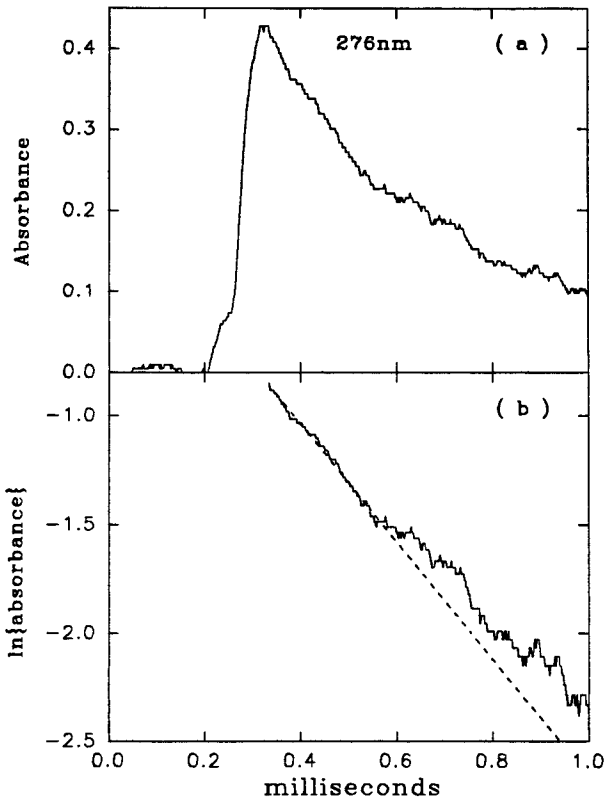

Figure 10. (a) Absorbance vs time (276 nm) during the thermal decomposition *i*-$CH_6(OH)NO_2$ at 1034 K. The first and second rises in absorbance are due to the density and temperature increases developed by the incident and reflected shock waves, respectively. Total pressure = 4.8 atm. [*i*-$CH_6(OH)NO_2$] = 5.1×10^{-7} mol/cm^3. (b) The logarithm of absorbance for of 2-nitropropanol vs time at 276 nm.

examined by Palo et al.[19] using laser-powered homogeneous pyrolysis (with a continuos-wave CO_2 laser and reactants photosensitized with SF_6). They then investigated the decomposition via surface pyrolysis in a micropulse reactor. They found that in the former case, the reaction proceeded entirely through C−NO_2 bond fission, whereas in the latter large amounts of additional products such as 2-nitropropene, aceto-

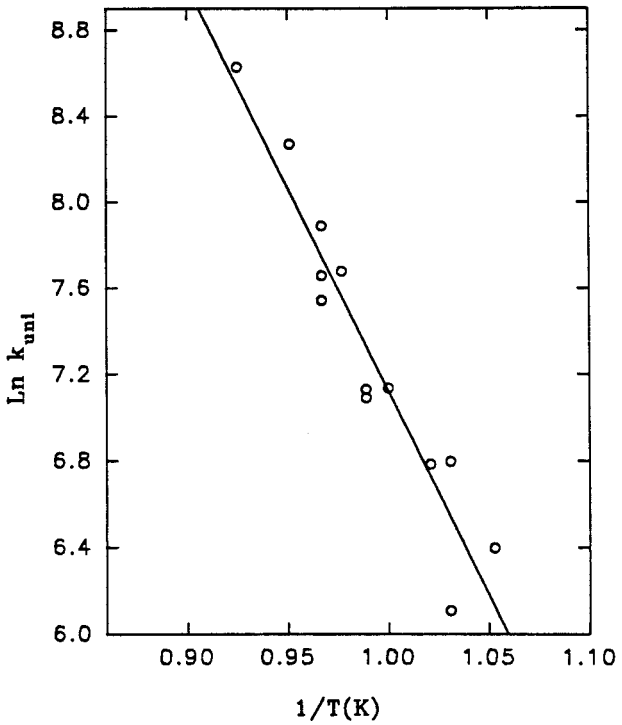

Figure 11. Arrhenius plot for the derived rate constants, for 2-nitropropanol. Total pressures at reflected shock condition are 4−5.3 atm. $[i\text{-}C_3H_6(OH)NO_2]_o$ is 3.5×10^{-7} −5.6×10^{-7} mol/cm^3. Symbols are experimental values and the solid line is the least-squares fit of the data.

nitrile, and acetone were generated. These indicate that unique routes are followed in surface promoted reactions. In contrast, Glänzer and Troe[10] studied this decomposition over the temperature range 915−1200 K at total gas concentration (mainly Ar) 7×10^{-6}−1.5×10^{-4} mol/cc. The conversion was followed spectrophotometrically. They deduced $k_\infty = 10^{15.5}$ exp{(−54 kcal/mol)/RT} s^{-1} and proposed that the reaction was entirely initiated by C−NO_2 bond fission, while the HONO elimination pathway was negligible. The transient behavior of NO_2 was monitored but its analysis proved to be difficult because of the lack of the knowledge of the secondary reactions. In a separate report[20] they suggested that C−NO_2 bond fission remained dominant even at low temperatures (e.g., 400 K).

A number of investigators[21−23] also studied the photodecomposition of 2-nitropropane. Radhakrishnan et al.[21] induced photodissociation with UV irradiation at 222, 249, and 308 nm under collision-free conditions and detected different sets of products. They hypothesized the following four pathways to account for their observations: Reactions 4 and 5 may be

$$(CH_3)_2CHNO_2 \rightarrow C_3H_6NO + OH \quad (3)$$
$$(CH_3)_2CHNO_2 \rightarrow C_3H_6 + NO + OH \quad (4)$$
$$(CH_3)_2CHNO_2 \rightarrow C_3H_6 + HONO \quad (5)$$
$$(CH_3)_2CHNO_2 \rightarrow C_3H_7 + NO_2 \quad (6)$$

identical, since HONO quickly dissociates to HO and NO; reaction 3 has not been proposed previously.

Wodtke et al.[13] induced infrared multiple-photon dissociation (IRMPD) of several nitroalkanes in molecular beams. Their experimental data revealed that the 2-nitropropane decomposed through both HONO elimination and C−NO_2 bond fission. The branching ratio (k_{HONO}/k_{C-N}) under their conditions was 0.5 in favor of C−N bond fission.

While most of the investigations discussed above focused on the initial steps of the dissociation, we are concerned with both the initial steps of the reaction and the subsequent secondary reactions that lead to the final products. A clear understanding of the decomposition mechanism of the overall decomposition process is critical for determining the fundamental kinetics of high explosives.

It is evident that there are two major routes for the thermal decomposition of 2-nitropropane: C−N bond fission and HONO five-center elimination. The latter appears to be the dominant reaction at low temperatures, while under our conditions the first step is primarily C−N bond fission

$$(CH_3)_2CHNO_2 \rightarrow C_3H_7\bullet + NO_2 \quad (7)$$

The $C_3H_7\bullet$ radical further dissociates to generate several sets of products, but primarily $CH_3CH{=}CH_2$ and H. Subsequent reactions of H with NO_2 and the parent compound initiate a sequence of secondary reactions. A complete mechanism for the conversion is presented in Table 1. To fully describe the pyrolysis over wide temperature and pressure ranges, we included in the mechanism as many steps as are plausible. The rate constants for most of the reactions are available in the literature, the NIST Chemical Kinetics Database developed by Mallard et al.[24] is the main reference for these constants. For steps for which there are no reported rate constants, we propose estimates based on analogous reactions. The five-center HONO elimination as the first step of pyrolysis is also included. Our recommended rate constant for this reaction is 10^{11} exp{(−41 kcal/mol)/RT} s^{-1}. The A factor is low, consistent with the postulate that the transition structure is a moderately rigid ring.

The rate equations for the mechanism in Table 1 were numerically integrated using the temperatures, pressures, and concentrations calculated for the reflected shock regime from the measured shock speeds. The computed results were then compared with the experimental data. The NO_2 profiles at various temperatures are adequately reproduced. Overall, the agreement between experiments and simulations is reasonably good. Typical curves are dashed lines in Figures 5 and 6. These profiles are similar to the ones computed for the thermal decomposition of nitromethane, but they differ markedly from those recorded for 1,3,3-trinitroazetidine (TNAZ). In the case of TNAZ, there are not sufficient reactive intermediates to completely consume the excess NO_2. However, in all of these systems, the main NO_2 consuming step is the reaction between H and NO_2. Note that there are a number of secondary reactions that consume 2-nitropropane (reactions 9, 10, 23, 80, and 81), but their contributions are small (less than 10%); the simulated 2-nitroproane decay curve remains first order, but deviates somewhat from the predicted curve from the first order rate constant in eq 1.

The mechanism in Table 1 reproduces well the distributions of major products. The results for $CH_3CH{=}CH_2$, NO, CO, CH_3CHO, C_2H_4, and $(CH_3)_2CO$ are shown in Figures 7 and 8. The symbols in the figures are experimental values and the solid lines are numerical simulations based on the proposed mechanism. The most serious discrepancy between experiment and simulation appears for CH_2O; refer to Figure 9. The computed trend is probably correct because the measured concentrations are subjected to large errors. The amount of CH_2O is very small and its presence was estimated from a tiny peak in our GC plot (a shoulder of a large peak). Further refinement of our analytical methods is needed to clarify this point. Note that the proposed mechanism predicts traces of C_4H_{10}, C_3H_6, C_4H_8, and CH_3CN

TABLE 1: Decomposition Mechanism of 2-Nitropropane[a]

no.	reaction	A	n	E_a	ref
1	i-$C_3H_7NO_2 \rightarrow i$-$C_3H_7 + NO_2$	3.548E+14	0	54.2	*b*
2	i-$C_3H_7 \rightarrow CH_3CH{=}CH_2 + H$	2.000E+14	0	37.23	*b*
3	i-$C_3H_7 \rightarrow CH_3 + C_2H_4$	2.000E+13	0	42.12	26
4	i-$C_3H_7 + CH_3 \rightarrow i$-$C_4H_{10}$	5.636E+13	−0.68	0	27
5	i-$C_3H_7 + CH_3 \rightarrow CH_3CH{=}CH_2 + CH_4$	4.571E+12	0.68	0	27
6	i-$C_3H_7 + H \rightarrow CH_3CH{=}CH_2 + H_2$	3.631E+12	0	0	27
7	i-$C_3H_7 + H \rightarrow C_3H_8$	1.514E+14	0	0	28
8	$H + NO_2 \rightarrow HO + NO$	6.700E+13	0	0	*b*
9	i-$C_3H_7NO_2 + CH_3 \rightarrow i$-$C_3H_6NO_2 + CH_4$	1.380E+11	0	8.39	29
10	i-$C_3H_7NO_2 + OH \rightarrow i$-$C_3H_6NO_2 + H_2O$	2.500E+11	0	0	*b*
11	i-$C_3H_7 + OH \rightarrow CH_3CH{=}CH_2 + H_2O$	2.399E+13	0	0	27
12	i-$C_3H_7 + NO_2 \rightarrow i$-$C_3H_7ONO$	2.000E+13	0	0	*b*
13	i-$C_3H_7ONO \rightarrow i$-$C_3H_7O + NO$	1.581E+16	0	41.0	30
14	i-$C_3H_7O + NO \rightarrow i$-$C_3H_7ONO$	2.042E+13	0	0	31
15	i-$C_3H_7O + NO \rightarrow i$-$C_3H_7NO_2$	3.162E+13	0	0	32
16	i-$C_3H_7O + NO \rightarrow (CH_3)_2CO + HNO$	6.310E+12	0	0	31
17	i-$C_3H_7ONO \rightarrow (CH_3)_2CO + HNO$	1.995E+14	0	38.90	33
18	i-$C_3H_7ONO \rightarrow CH_3CH{=}CH_2 + HONO$	5.012E+12	0	37.90	33
19	$HONO + M \rightarrow HO + NO + M$	1.191E+21	−3.8	48.37	34
20	i-$C_3H_7O \rightarrow (CH_3)_2CO + H$	2.000E+14	0	21.50	35
21	i-$C_3H_7O \rightarrow CH_3CHO + CH_3$	1.000E+15	0	17.50	35
22	$CH_3CH{=}CH_2 + OH \rightarrow CH_2CH{=}CH + H_2O$	1.900E+11	2.0	2.78	36
23	i-$C_3H_7NO_2 + H \rightarrow i$-$C_3H_6NO_2 + H_2$	2.500E+12	0	0	*b*
24	i-$C_3H_7 + HNO \rightarrow C_3H_8 + NO$	1.000E+12	0	0	37
25	$CH_3O + NO_2 \rightarrow CH_2O + HONO$	4.000E+11	0	0	38
26	$CH_3CH{=}CH_2 + OH \rightarrow CH_2{=}CCH_3 + H_2O$	1.000E+11	0	0	*b*
27	$CH_3CH{=}CH_2 + H \rightarrow C_2H_4 + CH_3$	7.228E+12	0	1.30	36
28	$CH_3CH{=}CH_2 + H \rightarrow CH_2CH{=}CH + H_2$	5.984E+11	2.5	5.82	*b*
29	$CH_3CH{=}CH_2 + H \rightarrow n$-$C_3H_7$	7.228E+12	0	2.90	39
30	$CH_3CH{=}CH_2 + H \rightarrow i$-$C_3H_7$	1.300E+13	0	1.56	40
31	$CH_3CH{=}CH_2 + H \rightarrow CH_2{=}CCH_3 + H_2$	5.984E+11	2.5	5.82	40
32	$H + H + M \rightarrow H_2 + M$	2.188E+15	−1.0	0	41
33	$H + OH + M \rightarrow H_2O + M$	2.489E+17	−2.0	0	42
34	$CH_3 + CH_3 \rightarrow C_2H_6$	2.190E+15	−1	0	43
35	$HNO + HNO \rightarrow H_2O + N_2O$	6.000E+09	0	0	34
36	$HNO \rightarrow H + NO$	2.130E+14	0	43.0	34
37	$CH_3 + HNO \rightarrow CH_4 + NO$	2.000E+12	0	0	37
38	$OH + HNO \rightarrow H_2O + NO$	4.819E+13	0	0.99	34
39	$H + HNO \rightarrow H_2 + NO$	1.811E+13	0	0.993	34
40	$HNO + NO_2 \rightarrow HNO_2 + NO$	8.000E+12	0	0	*b*
41	$HNO + HCO \rightarrow NO + CH_2O$	6.030E+11	0	1.987	34
42	i-$C_3H_6NO_2 \rightarrow CH_3CH{=}CH_2 + NO_2$	1.000E+09	0	0	*b*
43	$CH_3CH{=}CH \rightarrow CH_3 + C_2H_2$	1.259E+13	0	33.40	26
44	$CH_3CH{=}CH \rightarrow CH_3C{\equiv}CH + H$	3.981E+12	0	36.50	26
45	$CH_3CHO + M \rightarrow CH_3 + HCO + M$	5.010E+12	0	31.40	42
46	$CH_2{=}CCH_3 \rightarrow CH_3C{\equiv}CH + H$	9.550E+12	0	46.11	44
47	$CH_3CHO \rightarrow CH_3 + HCO$	2.000E+15	0	79.10	45
48	$CH_3CHO + CH_3 \rightarrow CH_4 + CH_3CO$	1.790E+08	5.64	2.464	41
49	$CH_3CHO + OH \rightarrow CH_3CO + H_2O$	1.000E+13	0	0	45
50	$CH_3CHO + H \rightarrow CH_3CO + H_2$	4.000E+13	0	4.207	45
51	$CH_3CHO + NO_2 \rightarrow CH_3CO + HONO$	3.119E+11	0	27.09	46
52	$CH_3CO + M \rightarrow CH_3 + CO + M$	1.200E+15	0	12.52	45
53	$CH_3 + NO_2 \rightarrow CH_3O + NO$	1.300E+13	0	0	47
54	$CH_3O + M \rightarrow CH_2O + H + M$	1.110E+22	−7.5	22.592	54
55	$CH_3 + C_2H_4 \rightarrow CH_3CH{=}CH_2 + H$	7.079E+12	0	11.127	48
56	$H + NO \rightarrow HNO$	1.470E+14	−0.41	0	34
57	$CH_2O + H \rightarrow HCO + H_2$	3.467E+12	1.27	2.6407	*b*
58	$CH_2O + M \rightarrow CO + H_2 + M$	2.120E+15	0	35.01	49
59	$H + N_2O \rightarrow OH + N_2$	9.640E+13	0	15.10	34
60	i-$C_3H_6NO_2 \rightarrow CH_2O + CH_3CNOH$	1.000E+07	0	0	*b*
61	$CH_3CNOH \rightarrow CH_3CN + OH$	1.000E+06	0	0	*b*
62	$CH_3 + NO_2 + (M) \rightarrow CH_3NO_2 + (M)$	3.590E+20 (k_o)	−6	0	47
		2.070E+13 (k_∞)	−0.6	0	47
63	$CH_3NO_2 + (M) \rightarrow CH_3 + NO_2 + (M)$	1.259E+17 (k_o)	0	42.0	*b*
		1.780E+16 (k_∞)	0	58.5	*b*
64	n-$C_3H_7 + H_2 \rightarrow C_3H_8 + H$	1.9200E+10	2.48	9.14	27
65	$i-C_3H_7 + H_2 \rightarrow C_3H_8 + H$	4.5600E+10	3.28	8.67	27
66	$CH_3CO + H_2 \rightarrow CH_3CHO + H$	1.310E+11	1.82	17.61	42
67	$CH_3CH{=}CH_2 + CH_3CO \rightarrow CH_3CHO + CH_2CH{=}CH_2$	4.710E+07	2.00	16.24	36
68	$CH_2CH{=}CH_2 + H_2 \rightarrow CH_3CH{=}CH_2 + H$	8.390e+10	2.38	18.99	36
69	$CH_2CH{=}CH_2 + CH_3 \rightarrow n-C_4H_8$	2.000e+12	0	0	*b*
70	$CH_2CH{=}CH_2 + CH_3 \rightarrow i-C_4H_8$	2.000e+12	0	0	*b*
71	$CH_3CH{=}CH_2 + OH \rightarrow CH_3CHO + CH_3$	2.100e+11	0	0	*b*
72	$CH_3CH{=}CH_2 + OH \rightarrow CH_2O + C_2H_5$	1.000e+11	0	0	*b*

TABLE 1 (Continued)

no.	reaction	*A*	*n*	E_a	ref
73	$C_2H_5 \rightarrow H + C_2H_4$	4.310e+12	1.19	37.20	42
74	$CH_2CH{=}CH_2 + NO \rightarrow CH_2CHCH_2NO$	2.110e+12	0	0.813	26
75	$i{-}C_3H_7NO_2 \rightarrow HONO + CH_3CH{=}CH_2$	1.000e+11	0	41	*b*
76	$CH_2CH{=}CH_2 + CH_2CH{=}CH_2 \rightarrow CH_2CCH_2 + CH_3CH{=}CH_2$	8.430e+10	0	0.262	36
77	$CH_2CH{=}CH_2 + n\text{-}C_3H_7 \rightarrow C_6H_{12}$	2.050e+13	0	0.131	36
78	$CH_2CH{=}CH_2 + i{-}C_3H_7 \rightarrow CH_3CH{=}CH_2 + CH_3CH{=}CH_2$	3.120e+12	−0.35	0.131	36
79	$CH_2CHCH_2NO \rightarrow CH_2CH{=}CH_2 + NO$	1.000e+15	0	55.0	*b*
80	$i\text{-}C_3H_7NO_2 + H \rightarrow (CH_3)_2CHNO + OH$	8.000E+11	0	0	*b*
81	$i\text{-}C_3H_7NO_2 + H \rightarrow i\text{-}C_3H_7 + HONO$	8.000E+11	0	0	*b*

[a] Rate constants are in the form $k = A(T/298)^n \exp\{-E_a(\text{kcal/mol})_a/RT\}$ with the unit of $cm^3\ mol^{-1}\ s^{-1}$ for bimolecular reactions. The Troe center-broadening parameter for the reaction 64 and 65 is Fcent = $0.3732 \exp(-T/250) + 0.6268 \exp(-T/901)$. [b] Rate constant assigned in this report.

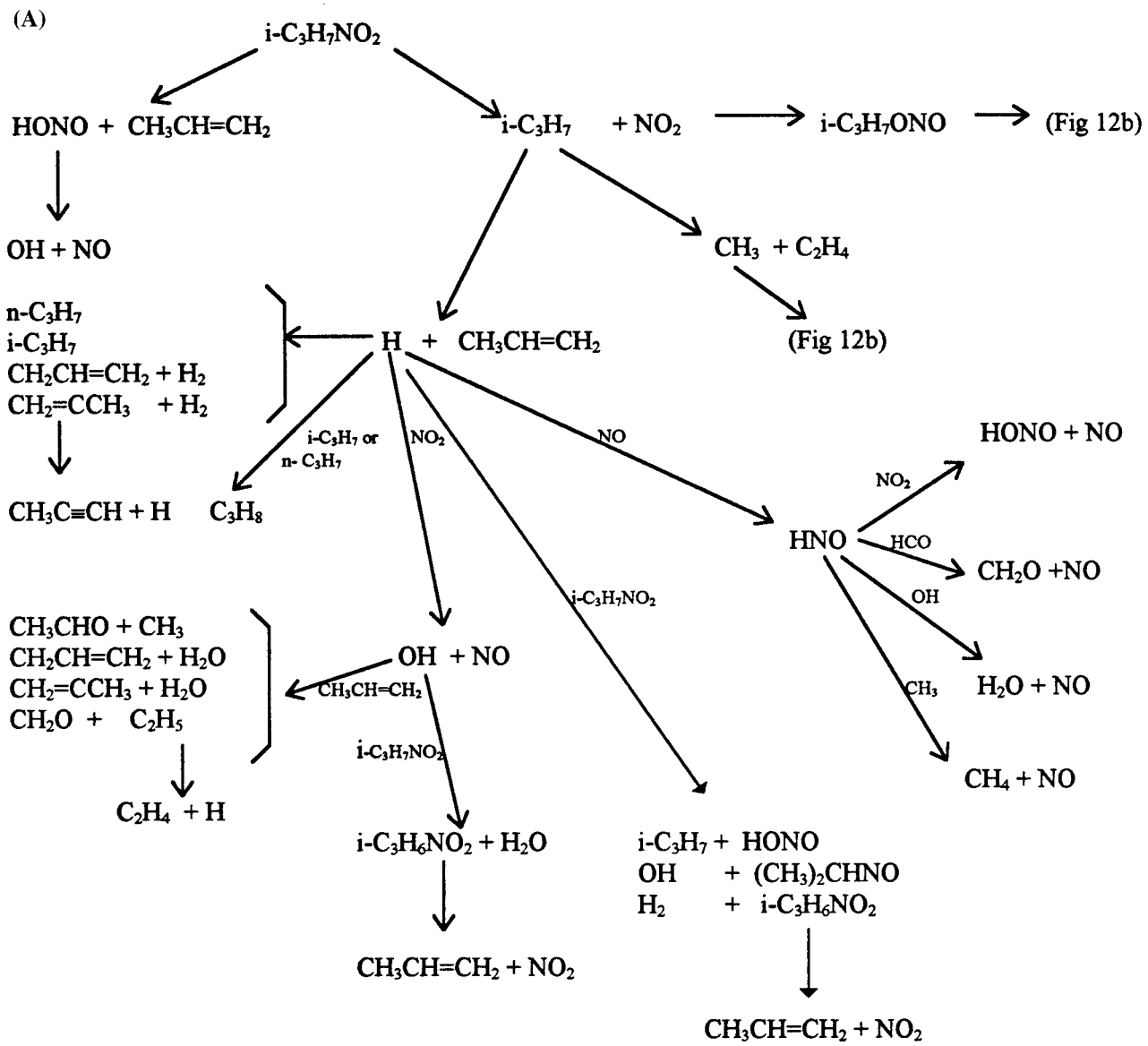

in the final product mixture. This is in agreement with our experiments. The mechanism also predicts a significant amount of $CH_2{=}CHCH_2NO$ in the final products, but its existence has not been established by the available analytical techniques.

The low *A* factor and activation energy for the thermal decomposition of 2-nitropropanol indicates that the first step of the reaction involves a tight transition structure. The most plausible step is a near concerted elimination of NO_2 and OH via a six member ring, an H-bonded transition structure that converts to $OH\cdots NO_2$ and $CH_3CH{=}CH_2$ (propylene). Then the transient species $OH\cdots NO_2$ quickly dissociates. The existence of a six-member ring that incorporates OH and NO_2 in compounds such as 2-nitropropanol has been extensively considered with respect to the possible presence of an intramolecular hydrogen bond.[52]

Secondary conversions may be induced by reactions between $i\text{-}C_3H_6(OH)NO_2$, NO_2, OH, and $CH_3CH{=}CH_2$. Note that the Arrhenius parameters for 2-nitropropanol are similar in magnitudes to those for the HONO elimination in the thermal decompositions of 2-nitropropane and nitroethane.[53]

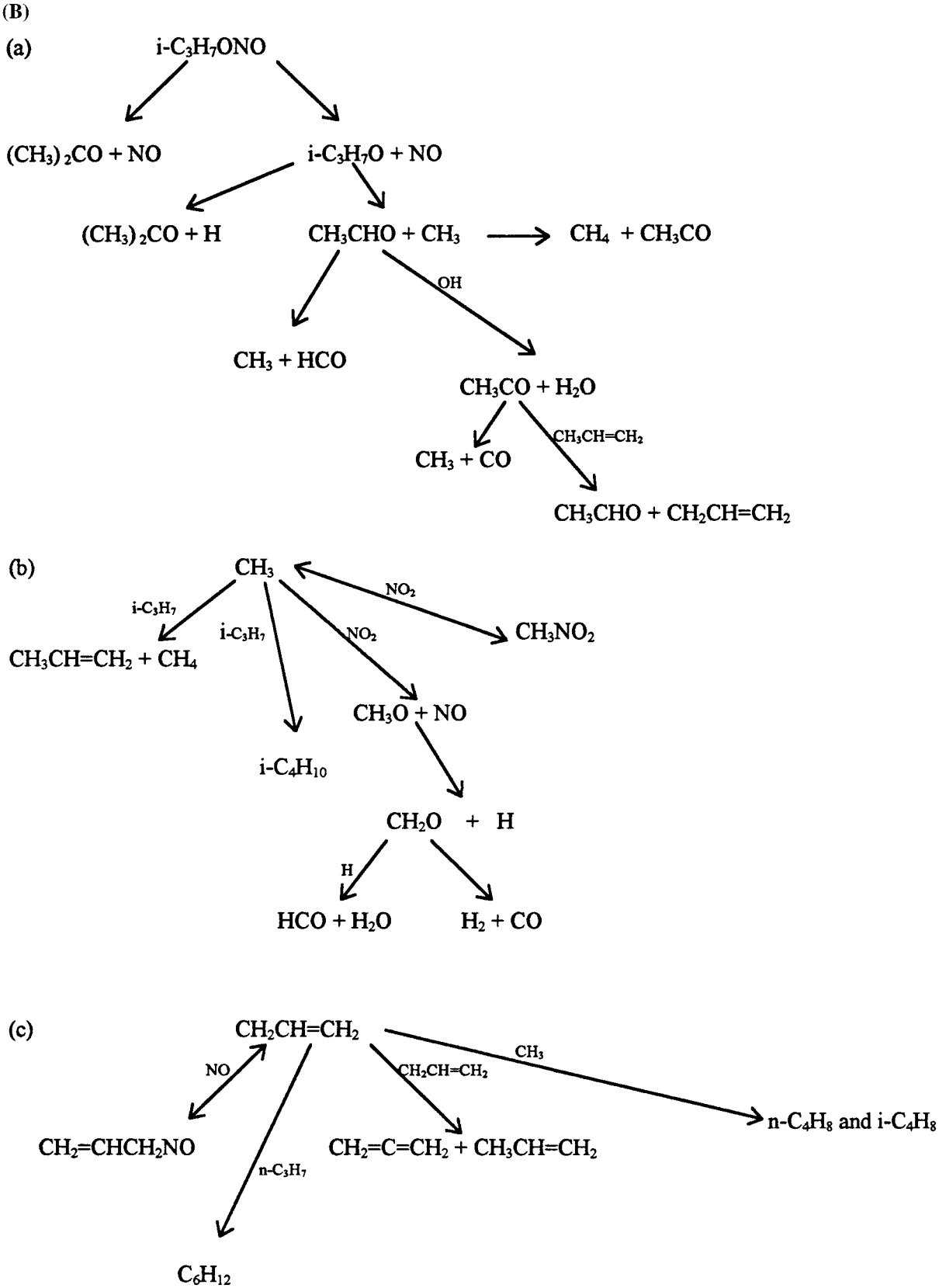

Figure 12. (A) Fragmentation and reaction sequence in the thermal decomposition of 2-nitropropane. Reactions initiated by the intermediates *i*-C_3H_7ONO, CH_3, and $CH_2CH{=}CH_2$ are shown in Figure 12B. (B) Reactions initiated by *i*-C_3H_7ONO, CH_3, and $CH_2CH{=}CH_2$ in the decomposition of 2-nitropropane.

Sensitivity Analysis

The mechanism in Table 1 was subjected to a sensitivity/principal component analysis as discussed previously.[6,25] The following criteria were used to determine the *importance* of any particular step in the mechanism: a step was considered *important* if it belongs to a reaction group with eigenvalues > 1.0×10^{-5}, and *unimportant* if it belongs to a reaction group

with an eigenvalue $< 1.0 \times 10^{-5}$. In any event, if the magnitude of the eigenvector of a reaction is less than 0.1, it is considered *unimportant*. The mechanism listed in Table 1 was first analyzed assuming that all the species in the mechanism were "observed", i.e., requiring that the reduced reaction mechanism from the analysis faithfully reproduces concentration profiles of all the inserted species. It was found that 16 steps (6, 14, 15, 16, 18, 24, 25, 32, 39, 43, 44, 47, 50, 51, 55, and 67) were unimportant during the entire decomposition process. The remaining mechanism was then further analyzed by considering only those species for which the concentrations reach at least 10^{-4} of $[i\text{-}C_3H_7NO_2]_o$ during part of the decomposition. These are $i\text{-}C_3H_7NO_2$, NO_2, $CH_3CH{=}CH_2$, C_2H_4, CH_4, H_2, C_3H_8, NO, H_2O, $(CH_3)_2CO$, HONO, CH_3CHO, $i\text{-}C_4H_8$, C_3H_5NO, CH_2CCH_2, CO, CH_3CN, CH_3NO_2, $n\text{-}C_4H_8$, and C_6H_{12}. It was found that seven more steps could also be omitted without altering the time evolution of the listed species: 11, 33, 34, 35, 59, 60, 78. The differences between the concentrations computed via the reduced and the full mechanism are less than 5%. A simplified mechanism tree is graphically presented in Figure 12. Note that the following atoms and free radicals are the most reactive species in this system: $i\text{-}C_3H_7$, H, CH_3, OH, and HNO. HONO elimination accounts for less than 20% of the total loss of $i\text{-}C_3H_7NO_2$ over the temperature range covered in this investigation.

Acknowledgment. The authors gratefully acknowledge the financial support for this investigation from Army Research Office under Grant No. DAAH04-95-1-0130.

References and Notes

(1) Olah, G. A.; Spuire, D. R. *Chemistry of Energetic Materials*; Academic Press: San Diego, 1991.
(2) Borman, S. *Chem. Eng. News* **1994**, Jan 17, 18−22.
(3) Adams, G. F.; Shaw, F. W., Jr. *Annu. Rev. Phys. Chem.* **1993**, *43*, 311.
(4) Bulusu, S. N., Ed. *Chemistry and Physics of Energetic Materials*; Kluwer Academic Publisher: The Netherlands, 1990.
(5) Zhao, X. S.; Hintsa, E.; Lee, Y. T. *J. Chem. Phys.* **1988**, *88*, 801.
(6) Zhang, Y.-X.; Bauer, S. H. *Int. J. Chem. Kinet.* **1999**, *31*, 655−673.
(7) Gardiner, W. C., Jr.; Walker, B. F.; Wakefield, C. B. In *Shock Waves in Chemistry*; Lifshitz, A., Ed.; Marcel Dekker Inc: New York, 1981.
(8) Huffman, R. Z.; Davidson, D. *J. Am. Chem. Soc.* **1959**, *81*, 2311.
(9) Zhang, Y.-X.; Bauer, S. H. *J. Phys. Chem. A* **1998**, *102*, 5846.
(10) Glänzer, K.; Troe, J. *Helv. Chim. Acta* **1973**, *56*, 1691.
(11) Nazin, C. M.; Manelis, G. B.; Dubovitskii, F. I. *Russ. Chem Rev.* **1968**, *37*, 603.
(12) Nazin, G. M.; Manelis, G. B. *Russ. Chem Rev.* **1994**, *63*, 314.
(13) Wodtke, A. M.; Hintsa, E. J.; Lee, Y. T. *J. Phys. Chem.* **1986**, *90*, 3549.
(14) Frejacquens, C. *Compt. Rend.* **1950**, *231*, 1061.
(15) Smith, T. E.; Calvert, J. G. *J. Phys. Chem.* **1959**, *63*, 1305.
(16) Waddington, C. J.; Ann Warriss, M. *J. Phys. Chem.* **1971**, *75*, 2427.
(17) Wilde, K. *Ind. Eng. Chem.* **1961**, *57*, 1750.
(18) Spokes, G. N.; Benson, S. W. *J. Am. Chem. Soc.* **1967**, *89*, 6030.
(19) Palo, J.; Faracova, M.; Kubat, P. *J. Chem. Soc., Faraday Trans. 1* **1984**, *80*, 1499.
(20) Glänzer, K.; Troe, J. *Recent Developments in Shock Tube Research, Proceedings of the 9th International Symposium*, 1973; p 743−748.
(21) Radhakrishnan, G.; Parr, T.; Witting, C. *Chem. Phys. Lett.* **1984**, *111*, 35.
(22) Mialocq, J. C.; Stephenson, J. C. *Chem. Phys.* **1986**, *106*, 281.
(23) Spears, K. G.; Brugge, S. P. *Chem. Phys. Lett.* **1973**, *54*, 373.
(24) Mallard, W. G. *NIST Chemical Kinetics Database*, Version 6.0, 1994.
(25) Zhang, Y.-X.; Bauer, S. H. *J. Phys. Chem. B* **1997**, *101*, 8717.
(26) Dean, A. M. *J. Phys. Chem.* **1985**, *89*, 4600.
(27) Tsang, W. *J. Phys. Chem. Ref. Data* **1988**, *17*, 887.
(28) Munk, J.; Pagsberg, P.; Ratajczak, E.; Sillesen, A. *Chem. Phys. Lett.* **1986**, *132*, 417.
(29) Ballod, A. P.; Titarchuk, T. A. *Kinet. Catal.* **1977**, *18*, 1359.
(30) Batt, L.; Milne, R. T. *Int. J. Chem. Kinet.* **1974**, *6*, 945.
(31) Batt, L.; Milne, R. T. *Int. J. Chem. Kinet.* **1977**, *9*, 141.
(32) Atkinson, R.; Baulch, D. L.; Cox, R. A.; Hampson, R. F., Jr.; Kerr, J. A.; Troe, J. *J. Phys. Chem. Ref. Data* **1992**, *21*, 1125−1568.
(33) Batt, L.; Islam, T. S. A.; Scott, H. *Int. J. Chem. Kinet.* **1978**, *10*, 1195.
(34) Tsang, W.; Herron, J. T. *J. Phys. Chem. Ref. Data* **1991**, *20*, 609−663.
(35) Heicklen, J. *Adv. Photochem.* **1988**, *14*, 177.
(36) Tsang, W. *J. Phys. Chem. Ref. Data* **1991**, *20*, 221−274.
(37) Laidler, K. J.; Sagert, N. H.; Wojciechowski, B. W. *Proc. R. Soc. London* **1962**, *270*, 254−266.
(38) Batt, L.; Milne, R. T.; McCulloch, R. D. *Int. J. Chem. Kinet.* **1977**, *9*, 567.
(39) Kerr, J. A.; Parsonage, M. J. *Evaluated kinetic data on gas-phase addition reactions: reactions of atoms and radicals with alkenes, alkynes and aromatic compounds*; Butterworths: London, 1972.
(40) Tsang, W. *Ind. Eng. Chem.* **1992**, *31*, 3−8.
(41) Baulch, D. L.; Cobos, C. J.; Cox, R. A.; Esser, C.; Frank, P.; Just, Th.; Kerr, J. A.; Pilling, M. J.; Troe, J.; Walker, R. W.; Warnatz, J. *J. Phys. Chem. Ref. Data* **1992**, *21*, 411−429.
(42) Tsang, W.; Hampson, R. F. *J. Phys. Chem. Ref. Data* **1986**, *15*, 1087.
(43) Slagle, I. R.; Gutman, D.; Davies, J. W.; Pilling, M. J. *J. Phys. Chem.* **1988**, *92*, 2455.
(44) Naroznik, M.; Niedzielski, J. *J. Photochem.* **1986**, *32*, 281.
(45) Warnatz, J. *Combustion Chemistry*; Gardiner, W. C., Jr., Ed.; Springer-Verlag: New York, 1984.
(46) Fifer, R. A. *Ber. Bunsen-Ges. Phys. Chem.* **1975**, *10*, 613.
(47) Glänzer, K.; Troe, J. *Ber. Bunsen-Ges. Phys. Chem.* **1974**, *78*, 182.
(48) MacKenzie, A. L.; Pacey, P. D.; Wimalasena, J. H. *Can. J. Chem.* **1984**, *62*, 1325.
(49) Miyauchi, T.; Mori, Y.; Imamura, A. *Symp. (Int.) Combust., (Proc.)* **1977**, *16*, 1073.
(50) Glänzer, K.; Troe, J. *Helv. Chim. Acta* **1972**, *55*, 2884.
(51) Tulloch, J. M.; Macpherson, M. T.; Morgan, C. A.; Pilling, M. J. *J. Phys. Chem.* **1982**, *86*, 3812.
(52) Ungnade, H. E.; Kissinger, L. W. *Tetrahedron* **1963**, 19 suppl. 1, p 121.
(53) Wilde, K. *Ind. Eng. Chem.* **1956**, *48*, 769.
(54) Hsu, D. S. Y.; Lin, M. C. *J. Eng. Mater. Technol.* **1985**, *3*, 95.